18

Characterization of Bone and Bone-Based Graft Materials Using FTIR Spectroscopy

M.M. Figueiredo, J.A.F. Gamelas and A.G. Martins
Chemical Engineering Department, University of Coimbra
Portugal

1. Introduction

Despite its static appearance, bone is a very dynamic living tissue that undergoes constant remodelling throughout life. After blood, bone is the second most commonly transplanted tissue in human medicine, and thus a thorough characterization of this material is of crucial importance. For instance, although it has been accepted that the whole bone strength is related to the bone mineral density (BMD), changes in this parameter often do not correlate with the probability of fracture. To improve the mechanical performance of bone, other material properties related to bone quality, and not only quantity, have to be investigated.

FTIR spectroscopy constitutes an excellent tool to characterize the bone matrix because its main components (carbonated hydroxyapatite and collagen) absorb infrared radiation at distinct, almost complementary, regions within the 500-4000 cm^{-1} range. This not only enables the study of the main contributions of each component separately, but also allows a further investigation of relevant parameters that mostly affect the structural and mechanical properties of bone, as well as its active metabolism. Furthermore, FTIR analysis, particularly when combined with microscopic technologies, enables the measurement of spatial variations in bone composition, allowing their correlation with micro-to-macro morpho-structural properties. In clinical studies, this allows the comparison between sound and diseased bone, and the analysis of therapeutic effects of drugs, among many other examples. On the other hand, FTIR spectroscopy is also commonly used to characterize bone grafts. Moreover, evidence that optimizing the osteointegration requires a fundamental knowledge of the material properties both of the bone graft and of the host bone tissue, has driven to extensive research on this subject, often supported by FTIR spectroscopy.

2. Bone composition and structure

Besides providing mechanical support, bone also plays diverse important metabolic functions. Even though bones possess various sizes and shapes, they share general chemical and structural features that, despite a static appearance on adult vertebrates, vary with and within species (Gamsjaeger et al., 2010; Mkukuma et al., 2004). In fact, among similar individuals, bone properties change with age, nutrition, hormonal equilibrium and health condition, in addition to other factors such as biomechanical environment (Aerssens et al., 1997; Fratzl et al., 2004). These variations are relatively restricted due to the constant remodelling processes that re-establish equilibrium. The bone turnover or remodelling, that consists on the resorption,

followed by the replacement of bone with little change in shape, acts as a dynamic response to multiple local and systemic factors (Robling et al., 2006). The bone metabolic functions are regulated by the combined action of two principal cell lineages: the bone forming cells (mainly osteoblasts and osteocytes) and bone resorption cells (osteoclats). Diverse enzymes and many other molecules, such as the important bone morphogenetic proteins (BMPs), participate in those dynamic cellular processes (Katz et al., 2009; Urist, 1965).

The composition of the extracellular matrix of bone, often described as a two-phase composite, consists of about 65 wt. % mineral component (carbonated hydroxyapatite) and 25 wt. % organic component (mainly type I collagen), being the remaining 10 wt. % water (Judas et al., 2005). These components have extremely different mechanical properties: the mineral is stiff and brittle while the (wet) protein is much more elastic and also much tougher than the mineral. Bone combines both the stiffness and the toughness in an unusual arrangement of material properties that result on a remarkable tensile strength and resistance against fracture (Fratzl et al., 2004; Rho et al., 1998).

The bone components are so tightly embedded that require the use of chemical procedures to obtain an effective separation of the mineral from the organic phase. The mineral component may be obtained using thermal treatment at high temperatures (calcination) to eliminate the organic component and conversely, the latter may be isolated using acid demineralization processes (Martins et al., 2008).

Mineral phase

Bone mineral is a poorly crystalline calcium-deficient apatite, with a Ca:P ratio that differs from 1.67, which is the theoretical value for pure hydroxyapatite [$Ca_{10}(PO_4)_6(OH)_2$]. The nonstoichiometric biological apatites contain several ion substitutions. For example, Na^+ and Mg^{2+} may substitute Ca^{2+} ions, HPO_4^{2-} ions may substitute phosphate ions, and Cl^- and F^- may replace OH^-. Additionally, carbonate ions, the most abundant substitutions (3-8 wt. %), may occupy either the OH^- (type A apatite) or PO_4^{3-} (type B apatite) positions in the crystal lattice. The mineral component of bone is usually closer to B-type apatite (Landi, 2003; Murugan et al., 2006).

The crystalline structure of carbonated hydroxyapatite belongs to the hexagonal system, although a portion of the bone mineral remains amorphous. In fact, the apatite crystals comprise two different environments: a non-apatitic hydrated domain, containing diverse labile and reactive ions, surrounds a relatively inert and more stable apatitic domain (Fig. 1) (Farlay et al., 2010). In the interface between these domains, labile anions (PO_4^{3-}, HPO_4^{2-} and CO_3^{2-}) and cations (Ca^{2+}, Mg^{2+}) are easily and reversibly exchangeable. During initial crystal formation, ionic exchange occurs and ions gradually incorporate into the interior unit cell. The maturation of the mineral is associated with reduction of labile non-apatitic environments while stable apatitic domains augment. Moreover, as bone mineral becomes more mature, it contains less structural defects, both the size and number of crystals increase and its composition becomes closer to the stoichiometric hydroxyapatite. For this reason, crystal maturity is often associated with crystallinity (that augments with crystal size and mineral perfection).

Organic phase

The organic matrix of bone consists of collagen and a series of non-collagenous proteins and lipids. About 85–90 wt. % of the total bone protein corresponds to Type I collagen fibers.

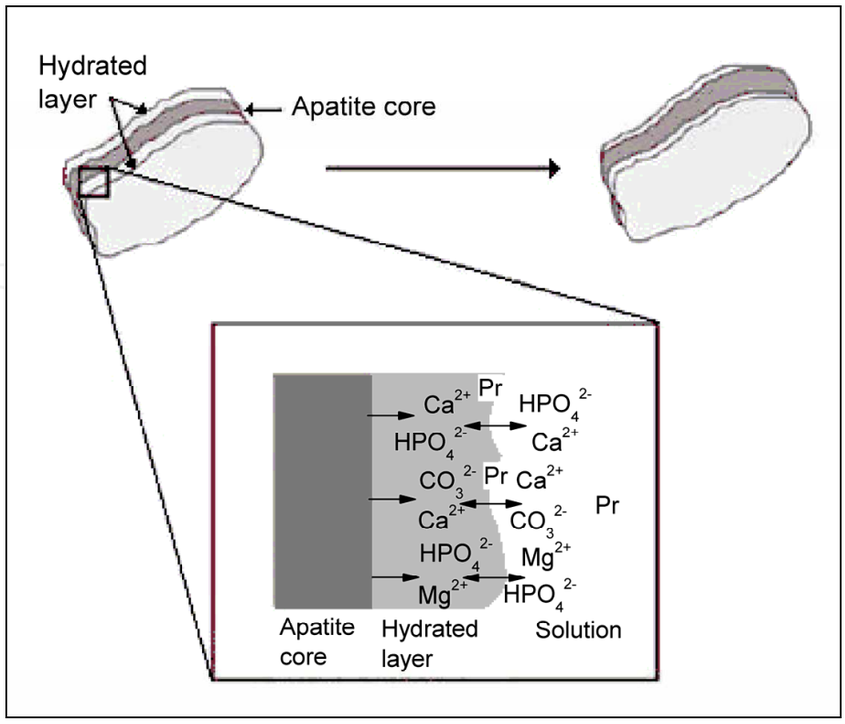

Fig. 1. Evolution of the apatite crystal and of the surrounding hydrated layer. During maturation and growth of the mineral, the apatitic domain of the crystal increases whereas the hydrated layer decreases, due to continuous ionic exchange between these domains and the solution bath. Soluble charged groups of proteins (Pr) can also participate in the ionic equilibrium of the non-apatitic domain (adapted from Farlay et al., 2010).

This principal component of the organic matrix of bone is a large fibrous protein with a highly repetitive amino acid sequence [Gly (glycine)–X–Y]n (often X is proline and Y is hydroxyproline). Other amino acids may also be found, such as alanine, lysine and hydroxylysine. These monomers are bound together by peptide bonds (between the carboxyl and amino groups of adjacent amino acids) constituting three polypeptide chains (two α1 and one α2 chains) that fold into a unique structure (Fig. 2). This consists of a single uninterrupted triple helix which represents more than 95% of the molecule (tropocollagen) and two non-helical domains (the telopeptides) containing the – COOH and – NH_2 terminals of the protein.

The integrity of the collagen molecule is attributed to the formation of intra- and inter-molecular cross-linking which contribute to the mechanical strength of the bone organic matrix (Eyre & Wu, 2005; Ottani et al., 2001; Saito & Marumo, 2009). Inter-molecular collagen cross-links can be divided into two types: lysine hydroxylase/lysyl oxidase-controlled cross-links (enzymatic cross-links) and glycation/oxidation-induced cross-links. In both cases, cross-linking sites are at specific Lys (lysine) or Hyl (hydroxylysine) residues of the collagen molecule. Concerning the first type, the enzymatic activity leads to the formation of Lys and Hyl aldehyde-derived covalent cross-links, in which a molecular fragment binds a telopeptide and a triple helix of adjacent molecules (divalent cross-link). As a consequence of chemical reactions and rearrangements, divalent cross-links may be converted into trivalent cross-links, in which a helix is bound to two telopeptides. As

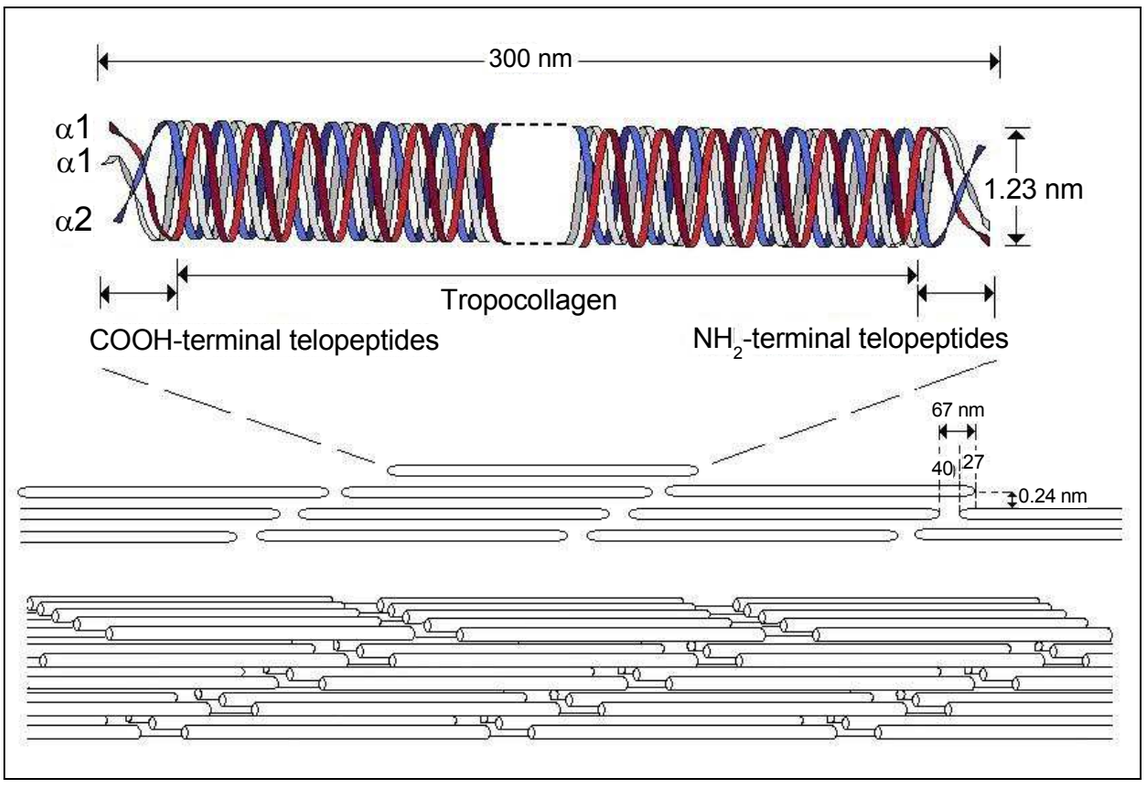

Fig. 2. Structure of the collagen molecule: three intertwined polypeptide chains (two α1 and one α2) constitute a major triple helical domain (tropocollagen) and two non-triple helical domains (telopeptides) at the –COOH and –NH_2 terminals of the protein. The typical staggered arrangement found in the collagen fibrils is displayed both in 2D and 3D configurations. The gap regions between the molecules are nucleation sites for hydroxyapatite.

suggested by the sequence of the mechanism of formation, divalent cross-links are classified as immature, whereas trivalent are considered as mature. These cross-links are also commonly named after their reactivity with sodium borohydride: typically, divalent cross-links are reducible fragments whereas trivalent are non-reducible. As for the second type, glycation cross-links, these are formed between collagen helices (telopeptides are not involved), being frequently associated with the ageing process that is generally deleterious to the function of the bone tissue. In fact, the extent and type of collagen cross-linking are known to change throughout life, leading to less flexible and less elastic properties. Besides the usual bone mass loss associated with age, the accumulation of glycation cross-links and of mature enzymatic cross-links in collagen is also thought to contribute to the fragility and brittleness of bone (Saito & Marumo, 2009; Viguet-Carrin et al., 2010).

Bone matrix structure

The structure of the mature bone matrix (Fig. 3) is highly organized on several hierarquical levels, starting with nanoscopic crystals of hydroxyapatite that are oriented and aligned within collagen fibrils (Fratzl et al., 2004; Olszta et al., 2007; Rho et al., 1998; Tzaphlidou, 2005; Viguet-Carrin et al., 2005). These result from the self-assembly of collagen molecules and mineral deposition, mainly in the regularly spaced gap regions of the organic structure

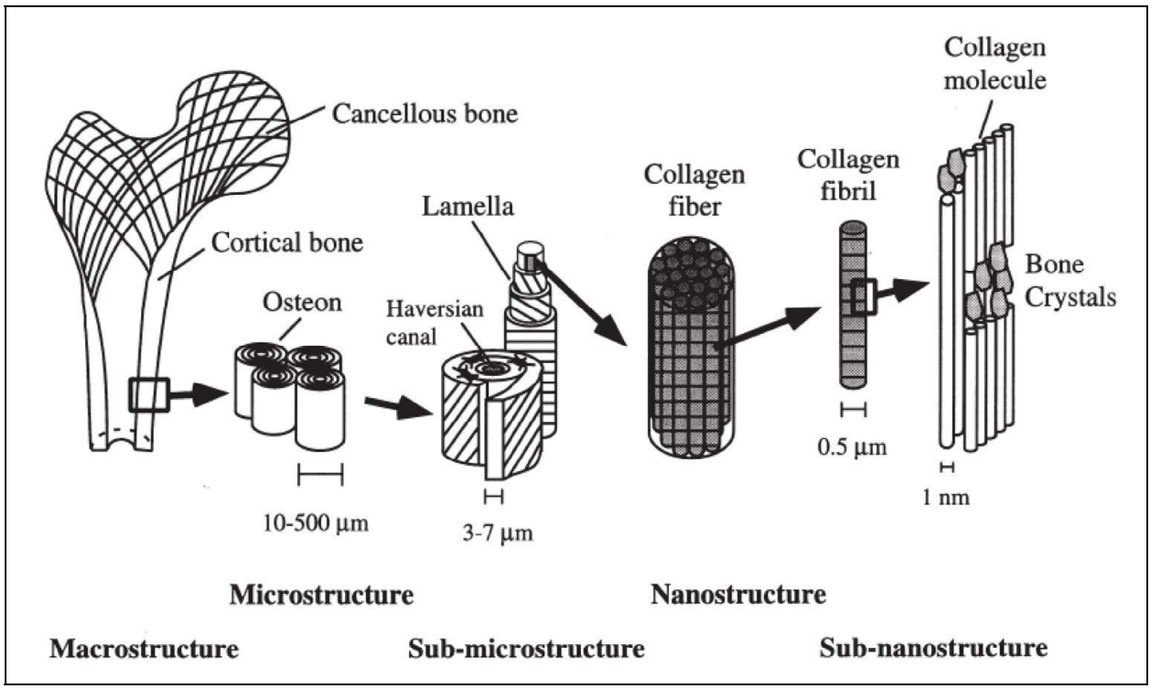

Fig. 3. Hierarquical structure of the bone matrix (from Rho et al., 1998).

(Fig. 2) (Nudelman et al., 2010). The association of the mineralized fibrils constitutes larger fibers which are layered in parallel arrangement forming lamellae with an alternate oriented "plywood" appearance (Goldman et al., 2005). Lamellar bone may be disposed concentrically around blood vessels, like rings of a tree, to form osteons (Havers Systems). This organization, from a nano to a macroscopic level, leads essentially to two distinct morphologies: compact bone, composed of densely packed osteons (Silva et al., 2005), and cancellous bone, wherein lamellae are assembled as spaced spicules (trabeculae), originating an interconnected microporous structure (Lozupone & Favia, 1990; Olszta et al., 2007). Compact bone is also called cortical because it always occupies a peripheral position relative to cancellous (or trabecular) bone.

It is interesting to perceive that each hierarchical structure of this anisotropic composite material is optimised to achieve a remarkable mechanical performance, from its basic building block (the mineralized collagen fibril wherein hydroxyapatite crystals have the long axis parallel to the longitudinal axis of the collagen molecules) to the tri-dimensional architecture of compact and cancellous bone. Moreover, each structural level may undergo minor but fundamental modifications, to better adapt and respond to various biomechanical forces (Ottani et al., 2001). As stated in a basic rule of skeletal biology known as Wolff´s law, "the bone´s morphology is a reflection of what function the bone has been built to do or adapted to perform".

3. FTIR spectroscopy applied to bone characterization

The Fourier transform infrared (FTIR) spectroscopy is based upon the absorption of IR radiation during vibrational transitions in covalently bound atoms. The frequencies and intensities of the infrared bands provide relevant information on the nature of the molecular

bonds, their environment and their relative content in the material being analysed. In some cases, some structural information regarding molecular conformations can also be obtained (Nyquist et al., 1997).

In order to obtain FTIR spectra, solid state samples in powdered form are often mixed with the infrared transparent KBr salt and prepared as pellets. Using FTIR in the transmission mode, the incident infrared radiation passes through the sample pellet and the spectrum corresponds to the transmitted fraction of the radiation. Alternatively, using the attenuated total reflection (ATR) mode, the solid samples can be analysed directly (without mixing with other substances) and the infrared spectrum corresponds mainly to the interaction up to about 2 μm depth from the surface of the sample.

In addition to the conventional FTIR spectroscopy, a microscopic analysis coupled to the vibrational spectra is also currently used to characterize bone samples, providing further insight into the correlation between structural and functional features. In fact, the introduction of the technique of infrared microspectroscopy (FTIRM) in 1988, followed by the development of the infrared imaging (FTIRI) from 1998, enabled to combine the advantages of hystomorphometry of the bone tissue with spectroscopy in the infrared range. Firstly, FTIRM allowed acquiring the sequential infrared mapping of a sampling area. Later, using focal plane array detector technologies, FTIRI enabled the simultaneous spectral acquisition in each detector pixel, representing an important progress both quantitative and qualitatively. In fact, FTIR imaging provides all the functionality of mapping but does so faster, with better spatial resolution and most importantly, with considerably better sensitivity than FTIRM. Nowadays, both techniques are regularly applied to the *in vitro* analysis of human tissues, namely bone samples (healthy, diseased and archeological bone), as well as animal models (Isaksson et al., 2010; Lebon et al., 2008; Marcott et al., 1998). Samples are usually prepared from thin cut sections that, for FTIRM/FTIRI analyses and in opposition to conventional histological analysis, do not require specific staining. However, samples may have to be fixed with appropriate solvents and embedded on a rigid support (often polymeric resins) and these procedures may cause some deviations of the infrared absorption bands relative to the direct analysis of the material (Aparicio et al., 2002; Paschalis et al., 2011). To overcome this interference, the thin sections may be analyzed in the ATR mode (that most frequently requires little or no sample preparation) but this option may cause some loss of spatial resolution due to intrinsic limitations of the technique (Agilent Technologies, 2011; Petibois et al., 2009).

3.1 FTIR spectrum of the bone matrix

The composite nature of the bone matrix becomes very clear when its FTIR spectrum is compared with those of the model compounds of its components, hydroxyapatite and collagen (Fig. 4). In fact, the spectrum of bone exhibits all the most intense bands observed in the spectrum of hydroxyapatite (at 500-700 cm^{-1} and 900-1200 cm^{-1}) and that of collagen (in the 1200-1700 cm^{-1} and 2800-3700 cm^{-1} regions), being nearly coincident with the sum of the respective profiles. Nevertheless, there are some new bands (namely at around 870 cm^{-1} and 1400-1450 cm^{-1}) originated from carbonate substitutions in the crystal lattice of hydroxyapatite.

From the detailed spectral assignments presented in Table 1, some bands must be discussed, particularly in the 500-1700 cm^{-1} region of the spectrum of bone. The most intense bands are

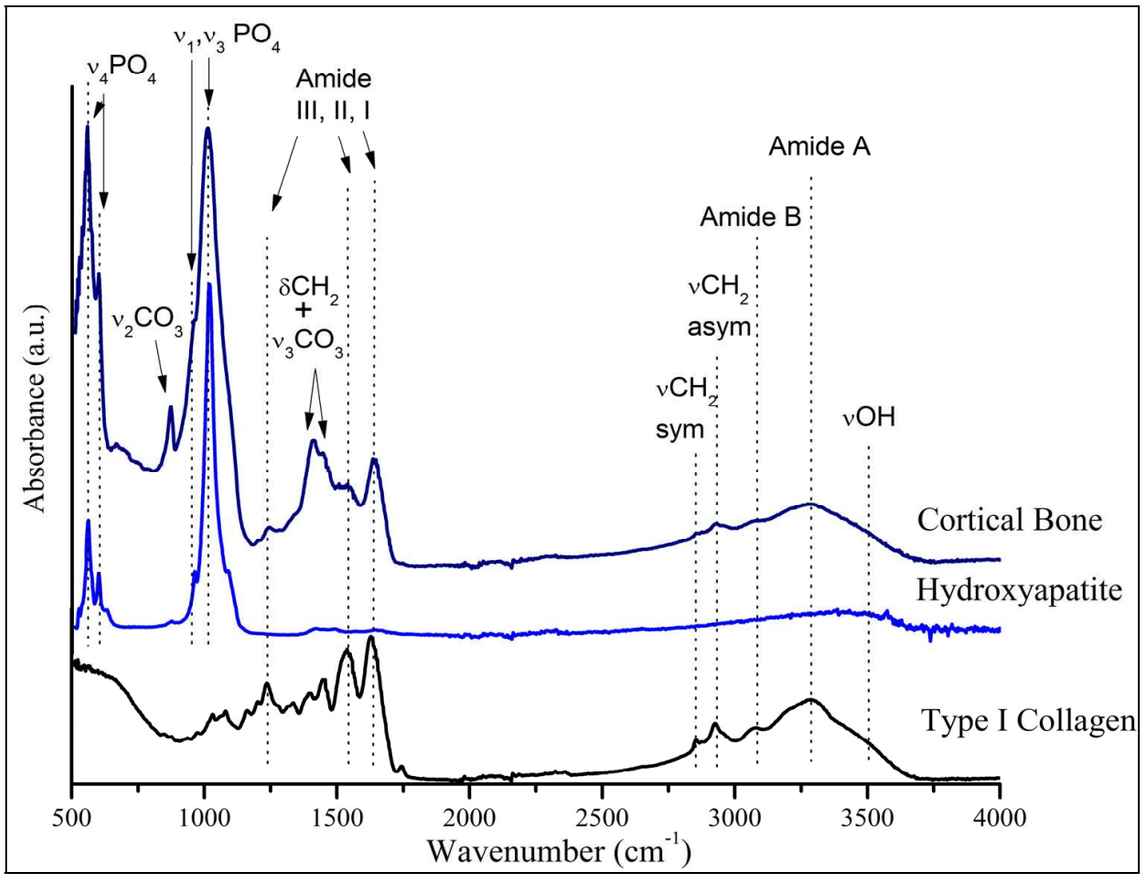

Fig. 4. Typical FTIR spectra of bone, hydroxyapatite and collagen showing the vibrational assignments of the most significant bands.

originated from the mineral phase, in accordance to its larger proportion in the composite. In particular, the bands at 557 and 600 cm^{-1} correspond mainly to ν_4 PO_4^{3-} bending vibrations, despite some minor contribution from collagen (amide bands) in that region. Moreover, the absorptions at 961 and 1012 cm^{-1} correspond to the symmetric (ν_1) and asymmetric (ν_3) stretching of phosphate, respectively. Thus, most of the absorptions from phosphate vibrations are clearly observed both in the spectra of bone and of hydroxyapatite.

It should be also mentioned that acidic phosphate (HPO_4^{2-}), a frequent anionic substitution in the crystal lattice of hydroxyapatite, usually originates a band at *ca.* 1110 cm^{-1}, which is normally overlapped with that from ν_3 PO_4^{3-} vibration.

On the other hand, the collagen moiety of bone originates the typical Amide I and Amide II bands at 1634 and 1548 cm^{-1}, respectively. Furthermore, the bands at 1410 and 1445 cm^{-1} show a different profile and higher intensity in the spectrum of bone relative to its organic model compound. These bands correspond, in fact, to absorptions from CH_2 wagging and bending vibrations superimposed with those from asymmetric stretching (ν_3) vibrations of CO_3^{2-} groups, present as ionic substitutes in the apatite crystal. Carbonate also originates a band at *ca.* 870 cm^{-1}, which is assigned to the ν_2 bending vibration. This band is characteristic of a type B apatite.

Wavenumber (cm^{-1})	Vibration modes		
	Bone	Hydroxyapatite	Collagen
557	ν_4 PO_4^{3-} bend (mineral) +Amide (organic)	ν_4 PO_4^{3-} bend	500-750 cm^{-1} Amide IV-VII
600	ν_4 PO_4^{3-} bend (mineral) +Amide (organic)	ν_4 PO_4^{3-} bend	
630	–	ν_4 PO_4^{3-} bend	
871	ν_2 CO_3^{2-} bend	–	–
961	ν_1 PO_4^{3-} sym stretch	ν_1 PO_4^{3-} sym stretch	–
1012	ν_3 PO_4^{3-} asym stretch	ν_3 PO_4^{3-} asym stretch	–
1250	Amide III		Amide III
1395	–	–	CH_2 wag
1410	ν_3 CO_3^{2-} (mineral)+ CH_2 wag (organic)	–	–
1445	CH_2 bend (organic)+ ν_3 CO_3^{2-} (mineral)	–	CH_2 bend
1548	Amide II	–	Amide II
1634	Amide I	–	Amide I
2850	CH_2 sym stretch	–	CH_2 sym stretch
2930	CH_2 asym stretch	–	CH_2 asym stretch
3072	Amide B	–	Amide B
3278	Amide A	–	Amide A
3500	ν OH	ν OH	ν OH

Table 1. Band assignments for the FTIR spectra of bone, hydroxyapatite and collagen, illustrated in Fig. 4.

As described, the infrared spectrum is a good diagnostic of the presence of phosphate (and also of carbonate) groups in the mineral component of bone, as well as the presence of amide groups in the organic fraction. In fact, these groups originate many typical absorption bands, as predicted theoretically.

Concerning the phosphate anions in tetrahedral geometry, there are four fundamental vibrations distributed as ν_1 (symmetric stretch), ν_2 (bend), ν_3 (asymmetric stretch), and ν_4 (bend) (Fig. 5) and these vibration modes (except ν_2) give rise to medium to strong bands (Nyquist et al., 1997). Typically, in hydroxyapatite, ν_1 (a non degenerate vibration mode) originates one intense band at around 960 cm^{-1}, and ν_3 and ν_4 (triply degenerate modes) originate up to three bands each in the 1000-1100 cm^{-1} and 500-650 cm^{-1} regions, respectively. Finally, the doubly degenerate mode ν_2 may be observed at less than 500 cm^{-1}.

Carbonate anions may also show up to four normal modes of vibration: symmetric stretch (ν_1), out-of-phase bending (ν_2), asymmetric stretch (ν_3) and in-plane CO_2 bending (ν_4) (Fig. 5). Whereas ν_2 is a non degenerate mode, both ν_3 and ν_4 are doubly degenerate and ν_1 is not

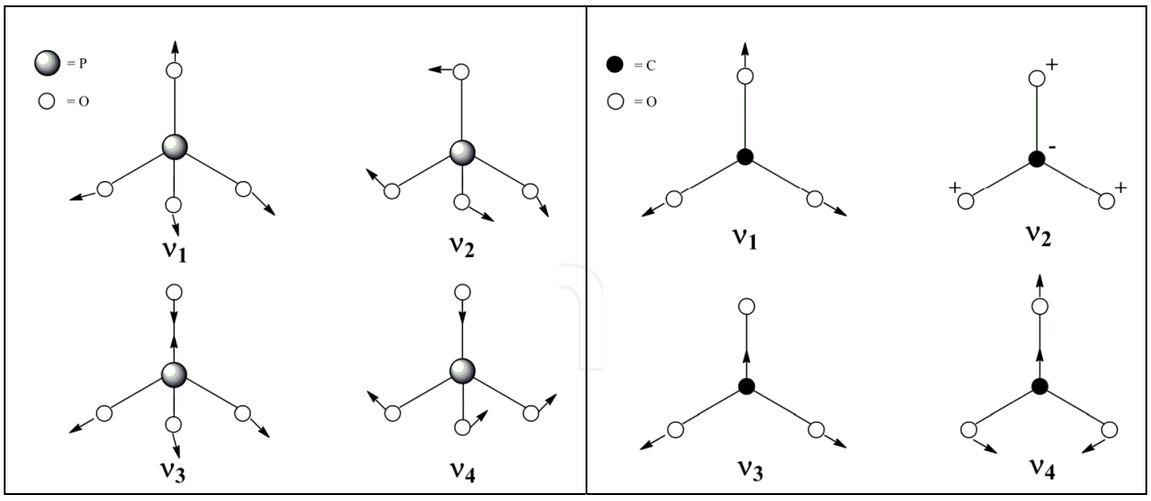

Fig. 5. Vibration modes for phosphate anions in tetrahedral symmetry and carbonate anions in D_{3h} symmetry (adapted from Nyquist et al., 1997).

an active vibration in the infrared because it does not change the dipole moment of the molecule (Nyquist et al., 1997). In carbonated apatites, the CO_3^{2-} characteristic bands appear at 870-880 cm^{-1} (ν_2, as a single band) and at 1400-1450 cm^{-1} (ν_3, usually as a double band). Depending on the type of carbonate substitution in the crystal lattice, bands may appear at slightly different wavenumbers: type *A* carbonated apatite is characterized by a ν_2 band at *ca.* 880 cm^{-1} and a ν_3 double band around 1450 and 1540 cm^{-1}, whereas type *B* configuration has these bands at about 870, 1430 and 1450 cm^{-1}, respectively (Fleet, 2009; Landi, 2003). The ν_2 band is often used to estimate the CO_3^{2-} content of the sample, by calculating the respective area underneath. Moreover, this band may also contain a component at *ca.* 865 cm^{-1}, due to the contribution of non-apatitic (labile) carbonate (Verdelis et al., 2007).

As for type I collagen, the organic component of bone, many vibrational bands are originated from the amide groups that constitute the peptide bonds of this protein. The characteristic vibrations of amide groups in collagen are usually combined modes designated as Amide I-VII, Amide A and Amide B (Chang & Tanaka, 2002; Garip & Severcan, 2010). The Amide I band, typically observed in the 1600-1700 cm^{-1} range, is the most intense absorption band in collagen. It results mainly from the C=O stretching vibration (with minor contribution from C-N stretch) and is directly related to the backbone conformation. Amide II, which originates a band at 1500-1600 cm^{-1} in collagen, is also conformationally sensitive and results mainly from an out-of-phase combination of N-H in-plane bending and C-N stretching vibrations of the peptide linkages. The Amide III band (1200-1300 cm^{-1}), just like the Amide II band, mainly arises from C–N stretch and N–H in-plane bending. The main difference between Amide II and III lies in the relative contribution of these modes for the respective mixed vibrations: whereas the N–H bending mode makes the larger contribution for the Amide II, the opposite occurs for the Amide III band. Amide IV is a C=O in-plane deformation and Amide V, VI and VII are out-of-plane motions (Roeges, 1994). The Amide A and Amide B bands, near 3300 cm^{-1} and 3100 cm^{-1} respectively, result from a Fermi resonance between the N-H stretch fundamental band and the overtone of amide II (Lee et al., 1999).

As demonstrated, the spectral contribution of the mineral and organic components to the overall FTIR spectrum of bone may be analyzed almost independently. This enables to estimate, for instance, the relative amount of mineral to organic matter and the proportion of carbonate in the bone apatite. Moreover, since high carbonate (and other ions) substitution correlates with a less mature mineral, FTIR data may also provide a measure of the crystal maturity based on the crystal stoichiometry. On the other hand, the maturity of the organic component of bone may also be evaluated through the analysis of specific amide bands from collagen.

Next section addresses the methodology usually applied to determine these and other parameters important for bone quality, demonstrating the extraordinary potential of FTIR analysis.

3.2 Assessing bone quality using FTIR

Bone quality is a broad term that encompasses factors affecting the geometric and material properties that contribute to fracture resistance. Geometric properties include the macroscopic geometry of the whole bone and the microscopic architecture of the trabeculae. On the other hand, material properties include the composition and arrangement of the primary constituents of bone tissue (collagen and mineral), as well as microdamage and microstructural discontinuities (Boskey, 2006, 2011; Paschalis et al., 1997). As mentioned earlier, the recent interest in bone quality arises from the fact that the traditional measurement of bone strength in clinical practice, namely bone densitometry, does not always reliably predict fracture risk. In fact, the bone mineral density (BMD) measurements primarily show the quantity of bone in the skeleton, overlooking more subtle aspects of bone's properties that may also contribute to its fragility. It is therefore important to understand alterations in bone that occur at the macro-, micro- and nanoscopic levels to determine what parameters affect bone quality and how they change with age or health condition.

FTIR spectroscopy, including FTIRM and FTIRI, providing information on all bone constituents at molecular level, represents an excellent tool to explore bone quality. The most frequently reported outcomes of FTIR related to bone material properties are the relative mineral and organic content, mineral maturity and crystallinity, carbonate substitution into the apatite lattice and collagen crosslinking. Because most of the bands of the bone spectrum are composed of several spectral components, deconvolution methods based on second derivative-spectroscopy and curve fitting have to be applied, being the results normally reported as a percentage of the area of specific underlying bands (Donnely 2010; Petibois et al., 2009). Hence, FTIR data are most commonly used for comparison purposes (between regions of the same sample, among samples or throughout time) rather than in absolute terms.

The proportion between the mineral and organic content in bone expresses its degree of mineralization and can be calculated from the ratio of the integrated area due to phosphate bands (usually ν_1, ν_3 in the 900-1200 cm^{-1} region) to that of a amide band (normally Amide I in the 1600-1700 cm^{-1} region). This ratio is an important indicator of the maturation or aging of bone and is linearly related to the bone mineral density (BMD) routinely measured in clinical medicine by dual energy X-ray absorptiometry. However, it should be pointed out that these parameters are not expressed in the same basis (BMD quantifies the amount of

mineral per volume whereas the ratio of the mentioned areas represents the amount of mineral per amount of collagen per volume analysed).

The mineral maturity is normally estimated based on sub-bands of the ν_1, ν_3 phosphate vibrations in the 900-1200 cm^{-1} region (Fig. 6). From deconvolution in this spectral range several individual peaks arise underneath the ν_3 band, being those at *ca.* 1020 and *ca.* 1030 cm^{-1} regarded as representative of specific chemical environments: typically, the sub-band at 1020 cm^{-1} is associated to nonstoichiometric apatites (containing HPO_4^{2-} and/or CO_3^{2-}) and that at 1030 cm^{-1}, to stoichiometric apatites. Given that the ratio of the areas of the sub-bands at 1020 and 1030 cm^{-1} has shown to decrease as mineral maturation proceeds, this ratio is often applied to evaluate the maturity of the bone apatite (Miller et al., 2001; Paschalis et al., 2011; Verdelis et al., 2007).

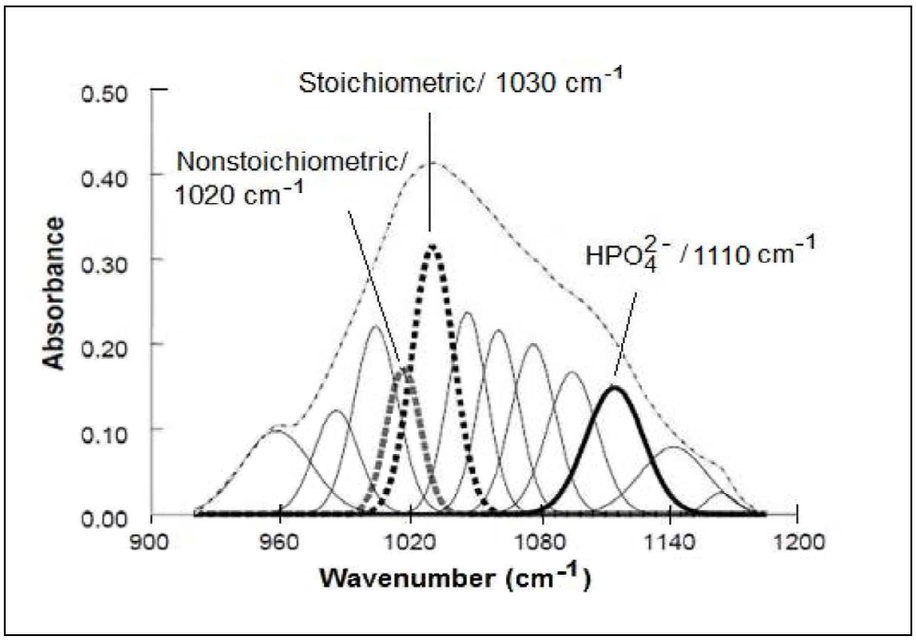

Fig. 6. Spectral region of the ν_1, ν_3 phosphate bands with underlying components revealed by curve-fitting. Sub-bands associated with the stoichiometry of the apatite (generally used for determination of mineral maturity) and the sub-band from HPO_4^{2-} (a common substitute in the apatite crystal) are highlighted (adapted from Verdelis, 2005).

It should be mentioned that since they evolve concomitantly, mineral maturity is normally associated with crystallinity. Thus, the simultaneous expression mineral maturity/ crystallinity is commonly employed, regardless these parameters do not refer to the same mineral properties (Farlay et al. 2011). Although the crystallinity of a mineral is typically calculated from X-ray diffraction, it has been suggested that in the particular case of hydroxyapatite, this parameter may also be determined from the well resolved FTIR band at *ca.* 600 cm^{-1} corresponding to a ν_4 phosphate vibration. Since the inverse of the full width at half maximum (1/FWHM) of this peak was found to be highly correlated with the state of crystallinity of the apatite (the narrower the peak, the higher the crystallinity), this ratio may be used as a crystallinity index. (Farlay et al. 2011). Moreover, it has been suggested that the ν_4 PO_4^{3-} peak at *ca.* 600 cm^{-1} is more reliable than the ν_3 PO_4^{3-} peak at *ca.* 1030 cm^{-1}, most

frequently associated with crystallinity (Shemesh, 1990). Finally, it should be emphasized that mineral maturity and crystallinity seem to be strongly correlated in synthetic apatites, but poorly correlated in human bone (especially in pathological bone). As expected in such a dynamic remodelling tissue, both parameters depend upon numerous factors including age, nutrition and health condition.

On the other hand, the maturity of the mineral phase is also related to the amount of substitutions in the crystal lattice of hydroxyapatite, being carbonate the most abundant in bone. Carbonate to phosphate ratio indicates the level of carbonate substitution and is calculated as the ratio of the carbonate band integrated area (850-890 cm^{-1}) to that of ν_1, ν_3 phosphate bands. This parameter seems a good indicator of the bone turnover and remodeling activity (Isaksson et al 2010). A combination of second derivative spectroscopy and curve fitting of the carbonate band (Fig. 7) reveals whether the carbonate has replaced hydroxide (A-type) or phosphate (B-type) in the apatite crystal, or is loosely attached to its surface (labile CO_3^{2-}). Considering that acidic phosphate is another eventual substitute in bone apatite, mineral maturity may also be estimated from the ratio between the overall ν_1, ν_3 phosphate band and the HPO_4^{2-} sub-band at *ca.* 1110 cm^{-1}.

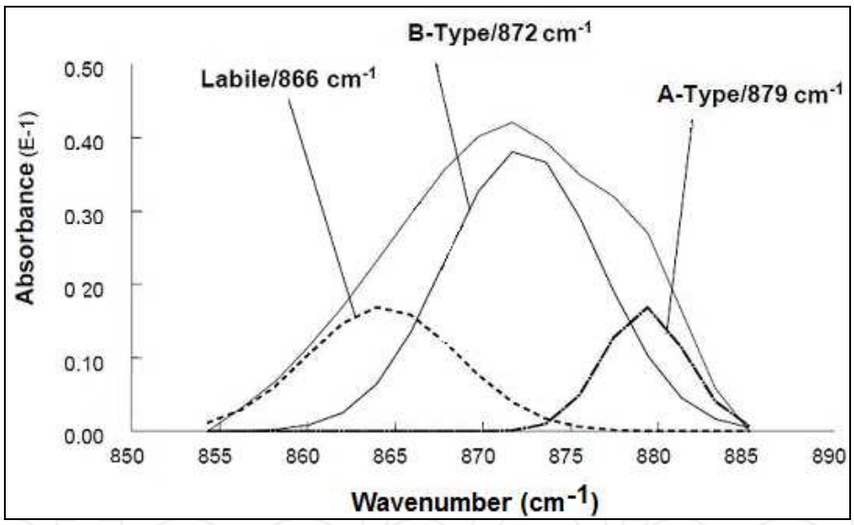

Fig. 7. Spectral region of the ν_2 carbonate band with components determined by curve-fitting, indicating the different types of carbonate substitution (adapted from Verdelis, 2005).

As previously mentioned, one of the most distinct features of type I collagen in mineralized tissues is its cross-linking chemistry. The intermolecular cross-linking provides high tensile strength and viscoelasticity to the fibrillar matrices. FTIR has been used to analyse the secondary structure of collagen, namely through the analysis of Amide I band. Information on protein structure may be obtained from the underlying bands of Amide I spectral region by resolution enhancement techniques (Fig. 8) (Paschalis et al., 2003). Of particular interest are two sub-bands: 1660 and 1690 cm^{-1}, related to the presence of non-reducible (mature) and reducible (immature) collagen cross-links, respectively. Thus, the ratio of the integrated areas of these bands (1660/1690) can be used as an indicator of the collagen maturity (Paschalis et al., 2011; Paschalis et al., 2001; Saito & Marumo, 2009).

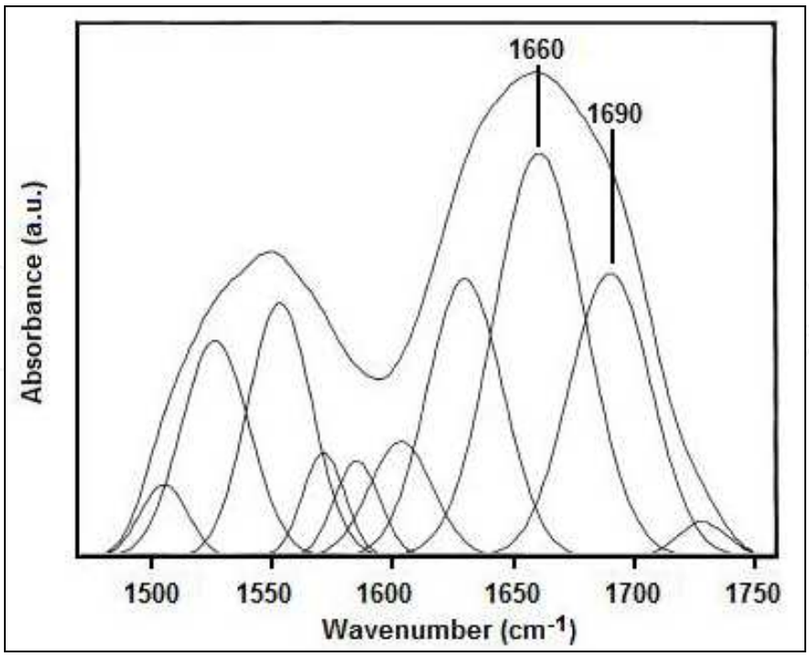

Fig. 8. Typical FTIR spectrum of collagen obtained from demineralized bovine bone in the region of Amide I and Amide II, resolved to its underlying components. Sub-bands at 1660 and 1690 cm^{-1} may be used to determine the maturity of collagen crosslinks (adapted from Paschalis et al., 2001).

Parameter	Ratio of the integrated areas or peaks intensities
Mineral/organic content	Phosphate bands (900-1200 cm^{-1})/amide I band (1600-1700 cm^{-1})
Mineral maturity	1030 cm^{-1} sub-band (stochiometric apatites)/1020 cm^{-1} sub-band (non-stochiometric)
CO_3^{2-}/PO_4^{3-} ratio	Carbonate bands (850-890 cm^{-1})/phosphate bands (900-1200 cm^{-1})
Type of CO_3^{2-}substitution	Ratio of integrated area or intensity of sub-bands at *ca.* 870 cm^{-1} (B-type carbonate), 880 cm^{-1} (A-type carbonate) and 865 cm^{-1} (labile carbonate)
Collagen maturity	1660 cm^{-1} sub-band (non-reducible/mature cross-links)/1690 cm^{-1} sub-band (reducible/immature cross-links)

Table 2. Relevant bone quality parameters derived from the FTIR data.

Table 2 summarizes the most important parameters generally used to evaluate bone quality derived from FTIR spectroscopy data. In addition, Figure 9 illustrates the spatial distribution of some of these parameters in thin sections of osteoporotic bone samples, as observed by FTIRI.

4. Characterization of bone-based graft materials using FTIR spectroscopy

Bone tissue posses a remarkable capacity to self-repair microdamages. Nevertheless, when a bone defect reaches a critical size, healing usually requires the introduction of grafting materials. Ideally, these should be able to provide a porous scaffold to enable cell invasion and attachment, and the subsequent formation of new bone.

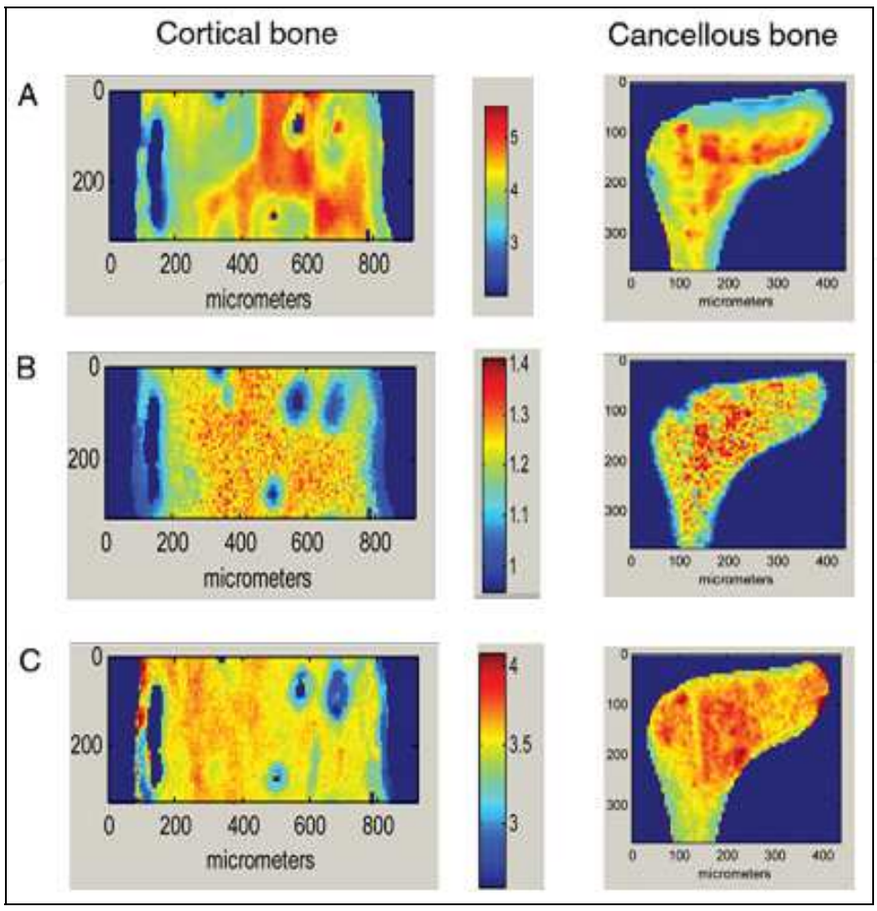

Fig. 9. Typical images obtained by FTIRI from an osteoporotic human iliac crest showing the spatial distribution of bone quality parameters in regions of cortical and cancellous bone: mineral/organic ratio (A), mineral maturity (B), and collagen maturity (C) (from Boskey, 2011).

A standard strategy applied when a bone loss occurs is using bone grafts which include autografts, allografts and xenografts (Bauer & Muschler, 2000; Torroni, 2009). An autograft consists of a tissue that is transferred from one site of the organism of an individual to a different location, an allograft represents a tissue transfer between individuals of the same species, and xenografts, between different species. Bone autografts, the "gold standard" in bone grafting procedures, have the advantage of no adverse immunological response and thus represent the best for inducing new bone formation. However, they are usually available in limited quantity (depending on donor site anatomy) and harvesting requires additional surgery, resulting in increased morbidity for the patient. Human allografts, which can be appropriately preserved in bone banks being thus available in greater abundance, represent a valuable alternative to autografts (Judas et al., 2005). Even so, the application of allografts is often limited due to uncertainty on compatibility and risk of disease transmission. Xenografts, most often of bovine or porcine origin, have no limitations regarding availability but, similarly to allogenous bone, can introduce risk of rejection and disease transmission.

Currently, the most common alternatives to bone-based grafts are synthetic biomaterials (often composites made of Ca/P ceramics and polymers) (Kikuchi et al., 2001). Although the raw materials of these composites are selected to fulfil many requirements (such as biocompatibility, osteoconductivity and non-toxicity), being often produced/modified to mimic the characteristics of natural bone, the best clinical results still derive from the application of autografts. Nonetheless, synthetic materials not only overcome most disadvantages of the natural bone grafts, but also provide more consistent and controllable properties. This is the case of diverse ceramic materials, namely hydroxyapatite, that besides being applied as components of composites, are also frequently used alone. In fact, synthetic hydroxyapatite is the most commonly used graft material mostly due to its resemblance with the bone mineral and similar osteocondutive potential. Synthetic hydroxyapatite, however, possesses some limitations including poor mechanical properties (specially when exposed to wet environments) and lack of osteoinductive properties. In addition, for the time being, synthetic apatites are not yet able to duplicate the composition and structure of the mineral component of bone, known to influence the grafts osteointegration. In fact, natural hydroxyapatite is nonstoichiometric and contains carbonate and other ions built into its structure. Although the presence of these ions is very low, they play a vital role in the biological reactions associated with bone metabolism (Barrere et al., 2006; Joschek et al., 2000). It has been shown that carbonate incorporation tends to decrease the crystallinity and to augment the solubility of hydroxyapatite, enhancing its biodegradation rate. Thus, synthetic hydroxyapatite is frequently modified chemically in order to include additional properties favorable to bone grafting.

A given type of graft can function by more than one mechanism. For instance, autografts are osteoconductive, osteoinductive and osteogenic whereas allografts and xenografts are mainly osteoconductive. Evidences that natural apatites also possess osteocondutive properties has stimulated their application as grafting materials, alone or combined with other materials. Currently, this mineral component of bone is usually obtained from calcined xenografts, being commercially available from different animal origins, under various formulations. On the other hand, in addition to osteocondutive properties, demineralized bone grafts have demonstrated to also possess osteoinductive capacities, which are mainly attributed to the exposure of bone morphogenetic proteins (BMPs) caused by the demineralization procedure. Thus, not only natural bone grafts, but also calcined and demineralized bone grafts constitute very important options that require extensive research regarding materials characterization, processing methods and application conditions, in order to help the prediction of their clinical outcome.

4.1 Bone-derived hydoxyapatite: Influence of the calcination temperature

One strategy to improve non-autograft materials while maintaining their advantages regarding their chemical and physical properties is to process natural bone, for example by heat treatment (Haberko et al., 2006; Joschek et al., 2000; Murugan et al., 2006; Ooi et al., 2007). Natural hydroxyapatite obtained in this way has the advantage of inheriting the chemical composition and structure of the raw material (Catanese et al., 1990; Etok et al., 2007; Murugan et al., 2003), being therefore an alternative solution for numerous applications based on its analogous synthetic products. As compared to allogeneic bone, hydroxyapatite derived from xenogeneic bone (usually of bovine origin) is considered a good option because it is easier to obtain at lower cost and is available in unlimited supply.

The problem that arises with heat treatment at elevated temperatures is that the biogenic composition and structure of bone mineral can change and this may affect the efficacy of this material (Etok et al., 2007; Hillera et al., 2003; Ooi et al., 2007). Although there is some controversy regarding the onset of chemical and structural changes as a consequence of heat treatment, it has been reported that changes in the mineral phase of bone are not significant until degradation and combustion of most of the more labile organic components occurs (around 500 ºC) (Etok et al., 2007; Mkukuma et al., 2004; Murugan et al., 2006; Ooi et al., 2007). Regarding sample mineralogy, it is generally accepted that heat treatment promotes the crystallinity of bone derived hydroxyapatite and increases the crystallite size (Etok et al., 2007; Hillera et al., 2003; Ooi et al., 2007).

A recent study concerning cortical bone samples of different origins (human and animal) subjected to different calcination temperatures (600, 900 and 1200 ºC) revealed that the calcination temperature highly affects the properties of the bone samples (Figueiredo et al., 2010). As expected, higher temperatures led to more pure forms of hydroxyapatite, with higher crystallinity degrees and larger crystallite sizes and a less porous structure. Furthermore, samples heated to the same temperature exhibited similar characteristics, regardless their origin.

FTIR spectra (Fig. 10) indicated that the organic constituents were no longer present in the samples calcined at 600 ºC, suggesting that this temperature is adequate to obtain protein-free samples. Moreover, these spectra have also revealed that, at this temperature, a carbonated apatite was obtained, being the carbonate removed from the mineral at higher temperatures. Furthermore, no new mineral phases were evident at higher temperatures, in good agreement with the results of thermal analysis, X-ray diffraction and additional confirmation by chemical analysis. Nevertheless, it has been reported that the apatite base

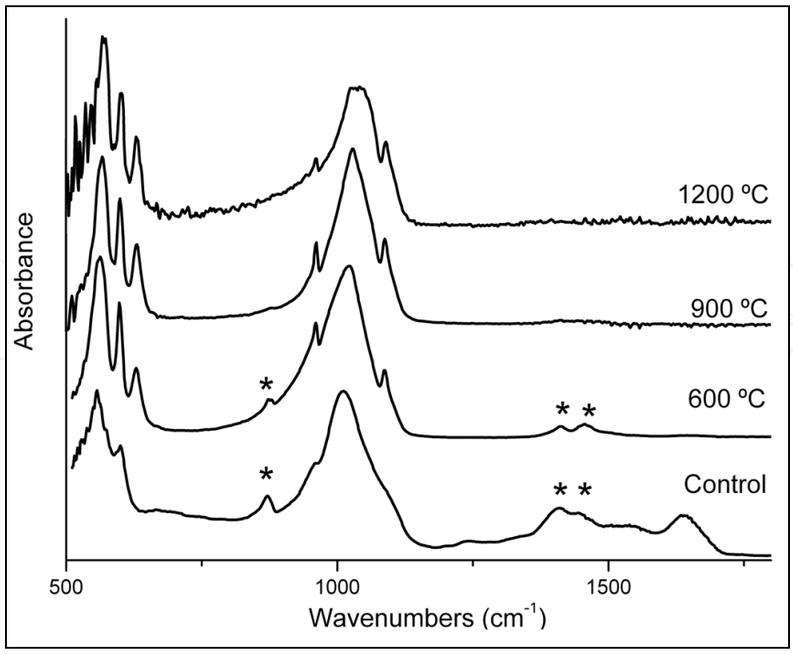

Fig. 10. FTIR spectra of human cortical bone before (control) and after calcination at 600, 900 and 1200 ºC. *Bands attributed to lattice carbonate vibrations (Figueiredo et al., 2010).

structure may be partially degraded by heating at temperatures higher than 800 ^{o}C, originating β-tricalcium phosphate ($Ca_3(PO_4)_2$) and/or CaO. However, the presence of these products in the mineral is better detected by X-ray diffraction than by FTIR spectroscopy (Etok et al., 2007; Haberko et al., 2006; Mkukuma et al., 2004; Ooi et al., 2007; Rogers & Daniels 2002).

SEM pictures (Fig. 11) of the human bone sample calcined at various temperatures showed that the samples surfaces no longer present the characteristic concentric lamellae around the Havers Canals, due to the elimination of collagen with heat treatment. Nonetheless, the basic microstructure of cortical bone (Havers Canals and osteocyte lacunar spaces, in particular) was preserved after calcination. Additionally, it was also apparent that the size of the apatite crystals increased with temperature, resulting on increased crystalinity (as confirmed by X-ray diffraction).

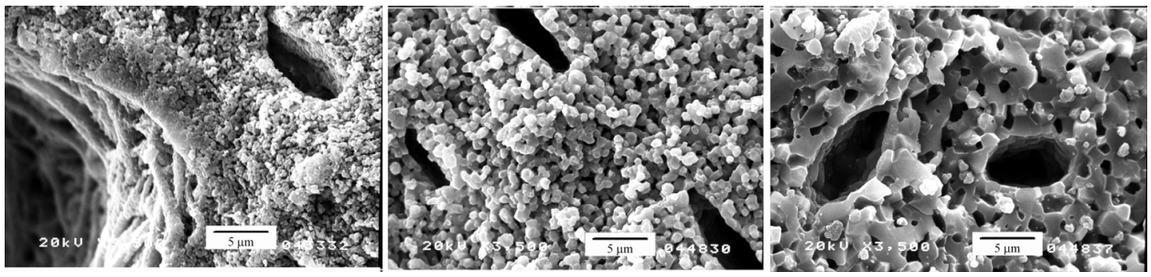

Fig. 11. Scanning Electron Microscopy images of human cortical bone calcined at 600, 900 and 1200 ^{o}C (from left to right) showing the increase in crystal size with temperature (Figueiredo et al. 2010).

Moreover, heat treatment also resulted in different porosity characteristics. Regarding porosity and pore size distribution, assessed by mercury intrusion (Fig. 12), it was clear that samples calcined at 600 ^{o}C exhibit the highest porosity, around 50%, which, for a compact bone, is quite relevant. However, as the heating temperature increases, the porous structure condenses, sintering at very high temperatures (1200 ^{o}C) and originating porosity values comparable to those of the non-calcined samples.

4.2 Demineralized bone matrix: Effect of the acid concentration

Demineralized bone matrix (DBM) is often applied in orthopedics, periodontics, oral and maxillofacial surgery because of its inherent osteoconductive and osteoinductive properties, generally related, as mentioned, to bone morphogenetic proteins (BMPs) (Bauer & Muschler, 2000; Eppley et al., 2005; Katz et al., 2009). In fact, as mineral is removed, the matrix associated BMPs become available rendering DBM grafts osteoinductive (Pietrzak et al., 2009). These grafts can be used either alone (Libin et al., 1975; Morone & Boden, 1998; Pietrzak et al., 2005) or in combination with bone marrow, autogenous bone graft, or other materials (Kim et al., 2002; Kucukkolbasi et al., 2009; Nade & Burwell, 1977). Additionally, DBM exhibits elastic features, being easily shaped to fill osteochondral lesions with different shapes and sizes (Costa et al., 2001).

Despite the extensive use of DBM, conflicting results have been published in the literature regarding its bone-inducing abilities. This may be a consequence of following different

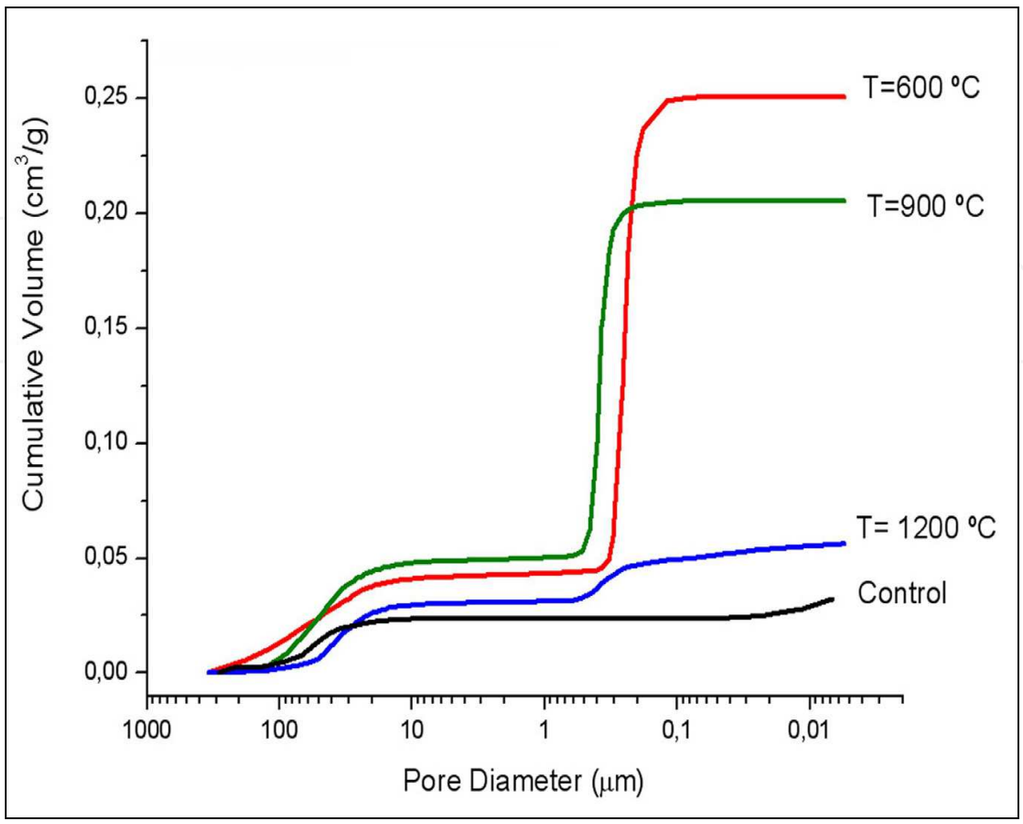

Fig. 12. Cumulative intrusion curve of human cortical bone, before (control) and after calcination at 600, 900 and 1200 ºC, measured by mercury porosimetry (Figueiredo et al., 2010).

demineralization procedures that naturally result in products with different properties (Bae et al., 2006; Eggert & Germain, 1979; Y. P. Lee et al., 2005; Lomas et al., 2001; Peterson et al., 2004). As reported in a recent study about BMPs depletion in particles of bovine cortical bone under acid exposure (0.25 and 0.5 M HCl) (Pietrzak et al., 2009), the availability of BMP-7 increases as demineralization occurs but, after reaching a maximum in the extraction bath, continuously declines. These results alert for the need to control the demineralization processing conditions. Normally, the process of bone demineralization is carried out by immersing the sample in a variety of strong and/or weak acids. In the case of using HCl (the most frequently used), the major inorganic constituent of bone (hydroxyapatite) reacts to form monocalcium phosphate and calcium chloride (Dorozhkin, 1997; Horneman et al., 2004).

FTIR has been used to monitor the bone demineralization process using HCl under different experimental conditions (acid concentrations and exposure times) (Figueiredo et al., 2011). Fig. 13 shows the FTIR spectra of bone samples (¼ of a ring of a human femoral diaphysis after being transversely cut into rings of approximately 1 cm width) submitted to demineralization with HCl 1.2 M for different periods of time. From the analysis of the FTIR spectra of the surface and of the core of the bone blocks, it was confirmed that the demineralization starts at the surface (absence of ν_1, ν_3 PO_4^{3-} bands and relative increase of the

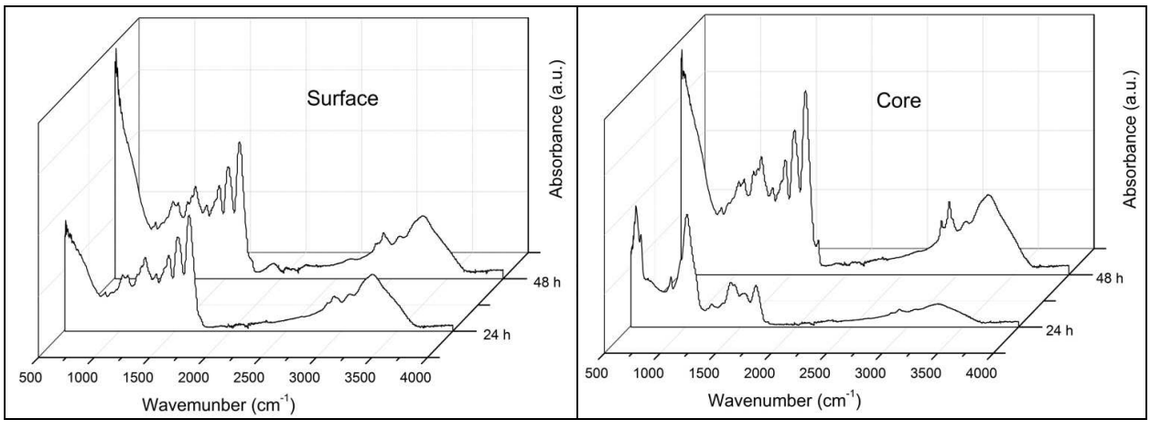

Fig. 13. FTIR spectra from the outer surface and from the core of the human bone samples after immersion in 1.2 M HCl for different time intervals. Demineralization proceeds from the surface into the core of the bone samples, as evidenced by the absence of phosphate bands and by the similarity with the spectrum of collagen.

collagen bands intensity) and progresses to the interior of the samples. These results support the concept of a diffusion model and agree with the proposed theory of the unreacted core during demineralization (Horneman et al., 2004; Lewandrowski et al., 1996, 1997).

This study was complemented with kinetic profiles and analysis of the samples´ structural modifications. As expected, increasing the acid concentration led to an increase in the demineralization rate, but not in a proportional way. In addition, microscopic observations demonstrated that despite the structural deformation resultant from demineralization, the basic bone microstructure was preserved. The loss of mineral led to a progressive reduction of mechanical strength and an increase of plastic properties (e.g. flexibility and elasticity) of the resultant material, mostly composed of collagen.

Although the deterioration of the organic component of bone was not examined in detail in this work, other studies using FTIR to analyse the effect of acids on the composition and structure of collagen during extraction from different tissues, may provide useful information on that subject. In fact, acid treatment of collagen samples was found to originate reduction of intermolecular cross-linking and hydrolysis of peptide bonds, as evidenced after curve-fitting in the spectral regions of the Amide I, II and III bands of collagen (Muyonga et al., 2004). These changes in collagen composition explained the observed loss of structural order. In addition, the amount and characteristics of the extracted fragments of collagen was related with the experimental conditions. These results agree with those from a FTIR study concerning the cross-linking of a collagen-hydroxyapatite nanocomposite with glutaraldehyde, as a model for the bone matrix (Chang & Tanaka, 2002). The spectral analysis showed that the increase of the cross-linking degree induces higher retaining of the organic content in the composite.

5. Conclusions

From the above, it is clear that FTIR spectroscopy is a sensitive and convenient tool to study the physicochemical modifications of bone composition regarding the mineral phase as well as the organic matrix. The detailed information provided by this technique is extremely

useful to study bone alterations that occur at macro-, micro- and nanoscopic levels, helping to reach a more consistent diagnostic.

Additionally, FTIR has been extensively used to characterize natural or synthetic graft materials, as well as to monitor the properties of the new bone formation. Furthermore, since the composition and the morphostructural parameters of a bone graft affect their biocompatibility, biodegradation and ultimately their osteointegration, the use of FTIR spectroscopy (including FTIRM and FTIRI) allows an interdisciplinary approach between chemists, molecular biologists and medical investigators.

6. References

Aerssens, J., Boonen, S., Joly, J., & Dequeker, J. (1997). Variations in trabecular bone composition with anatomical site and age: potential implications for bone quality assessment. *Journal of Endocrinology 155*, 411–421.

Agilent Technologies (2011). FTIR chemical imaging using focal plane array–based systems (Technical Overview ed.): Agilent Technologies, Inc.

Aparicio, S., Doty, S. B., Camacho, N. P., Paschalis, E. P., Spevak, L., Mendelsohn, R., et al. (2002). Optimal Methods for Processing Mineralized Tissues for Fourier Transform Infrared Microspectroscopy. *Calcified Tissue International 70*(5), 422-429.

Bae, H. W., Zhao, L., Kanim, L. E. A., Wong, P., Delamarter, R. B., & Dawson, E. G. (2006). Intervariability and intravariability of bone morphogenetic proteins in commercially available demineralized bone matrix products. *Spine, 31*(12), 1299–1306.

Barrere, F., van Blitterswijk, C. A., & de Groot, K. (2006). Bone regeneration: molecular and cellular interactions with calcium phosphate ceramics. *International Journal of Nanomedicine, 1*(3), 317-332.

Bauer, T. W., & Muschler, G. F. (2000). Bone graft materials. An overview of the basic science. *Clinical Orthopaedic Related Research, 371*, 10-27.

Boskey, A. (2006). Assessment of Bone Mineral and Matrix Using Backscatter Electron Imaging and FTIR Imaging. *Current Osteoporosis Reports, 4*, 71–75.

Boskey, A. (2011). Using bone quality to assess fracture risk. *American Association of Orthopaedic Surgeons Now, 5*(9).

Catanese, J., Featherstone, J. D. B., & Keaveny, T. M. (1990). Characterization of the mechanical and ultrastructural properties of heat-treated cortical bone for use as a bone substitute. *Journal of Biomedical Materials Research-Part A, 45*, 327-336.

Chang, M. C., & Tanaka, J. (2002). FT-IR study for hydroxyapatite/collagen nanocomposite cross-linked by glutaraldehyde. *Biomaterials, 23*, 4811–4818.

Costa, A., Oliveira, C., Leopizzi, N., & Amatuzzi, M. (2001). The use of demineralized bone matrix in the repair of osteochondral lesions. Experimental study in rabbits. *Acta Ortopédica Brasileira, 9*(4), 27-38.

Donnelly, E. (2010). Methods for Assessing Bone Quality: A Review. *Clinical Orthopaedics and Related Research, 469*(8), 2128-2138.

Dorozhkin, S. V. (1997). Surface Reactions of Apatite Dissolution. *Journal of Colloid Interface Science, 191*(2), 489–497.

Eggert, F. M., & Germain, J. P. (1979). Rapid Demineralization in Acidic Buffers. *Histochemistry, 59*, 215-224.

Eppley, B. L., Pietrzak, W. S., & Blanton, M. W. (2005). Allograft and alloplastic bone substitutes: a review of science and technology for the craniomaxillofacial surgeon. *Journal of Craniofacial Surgery, 16*(6), 981–989.

Etok, S. E., Valsami-Jones, E., Wess, T. J., Hiller, J. C., Maxwell, C. A., Rogers, K. D., et al. (2007). Structural and chemical changes of thermally treated bone apatite. *Journal of Materials Science, 42*(23), 9807-9816.

Eyre, D. R., & Wu, J.-J. (2005). Collagen cross-links. *Topics in Current Chemistry, 247*, 207–229.

Farlay, D., Panczer, G., Rey, C., Delmas, P. D., & Boivin, G. (2010). Mineral maturity and crystallinity index are distinct characteristics of bone mineral. *Journal of Bone and Mineral Metabolism, 28*(4), 433-445.

Figueiredo, M., Cunha, S., Martins, G., Freitas, J., Judas, F., & Figueiredo, H. (2011). Influence of hydrochloric acid concentration on the demineralization of cortical bone. *Chemical Engineering Research and Design, 89*(1), 116-124.

Figueiredo, M., Fernando, A., Martins, G., Freitas, J., Judas, F., & Figueiredo, H. (2010). Effect of the calcination temperature on the composition and microstructure of hydroxyapatite derived from human and animal bone. *Ceramics International, 36*(8), 2383-2393.

Fleet, M. E. (2009). Infrared spectra of carbonate apatites: v2-Region bands. *Biomaterials, 30*(8), 1473-1481.

Fratzl, P., Gupta, H. S., Paschalis, E. P., & Roschger, P. (2004). Structure and mechanical quality of the collagen/mineral nano-composite in bone. *Journal of Materials Chemistry, 14*(14), 2115.

Gamsjaeger, S., Masic, A., Roschger, P., Kazanci, M., Dunlop, J. W. C., Klaushofer, K., et al. (2010). Cortical bone composition and orientation as a function of animal and tissue age in mice by Raman spectroscopy. *Bone, 47*(2), 392-399.

Garip, S., & Severcan, F. (2010). Determination of simvastatin-induced changes in bone composition and structure by Fourier transform infrared spectroscopy in rat animal model. *Journal of Pharmaceutical and Biomedical Analysis, 52*(4), 580-588.

Goldman, H. M., Bromage, T. G., Thomas, C. D. L., & Clement, J. G. (2003). Preferred collagen fiber orientation in the human mid-shaft femur. *Anatomic Record Part A – Discoveries in Molecular Cellular and Evolutionary Biology, 272A*, 434-445.

Haberko, K., Bucko, M., Brzezinskamiecznik, J., Haberko, M., Mozgawa, W., Panz, T., et al. (2006). Natural hydroxyapatite—its behaviour during heat treatment. *Journal of the European Ceramic Society, 26*(4-5), 537-542.

Hillera, J. C., Thompson, T. J. U., Evison, M. P., Chamberlain, A. T., & Wess, T. J. (2003). Bone mineral change during experimental heating: an X-ray scattering investigation. *Biomaterials, 24*, 5091–5097.

Horneman, D. A., Ottens, M., Hoorneman, M., van der Wielen, L. A. M., & Tesson, M. (2004). Reaction and diffusion during demineralization of animal bone. *AIChE Journal, 50*(11), 2682-2690.

Isaksson, H., Turunen, M. J., Rieppo, L., Saarakkala, S., Tamminen, I. S., Rieppo, J., et al. (2010). Infrared Spectroscopy Indicates Altered Bone Turnover and Remodeling Activity in Renal Osteodystrophy. *Journal of Bone and Mineral Research, 25*(6), 1360-1366.

Joschek, S., Nies, B., Krotz, R., & Gopferich, A. (2000). Chemical and physicochemical characterization of porous hydroxyapatite ceramics made of natural bone. *Biomaterials, 21*, 1645-1658.

Judas, F., Teixeira, L., & Proença, A. (2005). Coimbra University Hospitals' Bone and Tissue Bank: twenty-two years of experience. *Transplantation Proceedings, 37*, 2799–2801.

Katz, J. M., Nataraj, C., Jaw, R., Deigl, E., & Bursac, P. (2009). Demineralized bone matrix as an osteoinductive biomaterial andin vitropredictors of its biological potential. *Journal of Biomedical Materials Research Part B: Applied Biomaterials, 89B*(1), 127-134.

Kikuchi, M., Itoh, S., Ichinose, S., Shinomiya, K., & Tanaka, J. (2001). Self-organization mechanism in a bone-like hydroxyapatite/collagen nanocomposite synthesized *in vitro* and its biological reaction *in vivo*. *Biomaterials 22*, 1705-1711.

Kim, S. G., Kim, W. K., Park, J. C., & Kim, H. J. (2002). A comparative study of osseointegration of Avana implants in a demineralized freezedried bone alone or with platelet-rich plasma. *Journal of Oral and Maxillofacial Surgery, 60*, 1018–1025.

Kucukkolbasi, H., Mutlu, N., Isik, K., Celik, I., & Oznurlu, Y. (2009). Histological evaluation of the effects of bioglass, hydroxyapatite, or demineralized freeze-dried bone, grafted alone or as composites, on the healing of tibial defects in rabbits. *Saudi Medical Journal, 30*(3), 329-333.

Landi, E. (2003). Carbonated hydroxyapatite as bone substitute. *Journal of the European Ceramic Society, 23*(15), 2931-2937.

Lebon, M., Reiche, I., Froehlich, F., Bahain, J. J., & Falgueres, C. (2008). Characterization of archaeological burnt bones: contribution of a new analytical protocol based on derivative FTIR spectroscopy and curve fitting of the υ_1 ν_3 PO_4 domain. *Analytical and Bioanalytical Chemistry, 392*(7-8), 1479-1488.

Lee, S.-H., Mirkin, N. G., & Krimm, S. (1999). A quantitative anharmonic analysis of the amide A band in α-helical poly(L-alanine). *Biopolymers, 49*, 195–207.

Lee, Y. P., Jo, M., Luna, M., Chien, B., Lieberman, J. R., & Wang, J. C. (2005). The efficacy of different commercially available demineralized bone matrix substances in an athymic rat model. *Journal of Spinal Disorder Technology, 18*(5), 439–444.

Lewandrowski, K. U., Tomford, W. W., Michaud, N. A., Schomacker, K. T., & Deutsch, T. F. (1997). An electron microscopic study on the process of acid demineralization of cortical bone. *Calcified Tissue International, 61*, 294–297.

Lewandrowski, K. U., Venugopalan, V., Tomford, W. W., Schomacker, K. T., Mankin, H. J., & Deutsch, T. F. (1996). Kinetics of cortical bone demineralization: controlled demineralization - a new method for modifying cortical bone allografts. *Journal of Biomedical Materials Research Part B: Applied Biomaterials, 11*(3), 365-372.

Libin, B. M., Ward, H. L., & Fishman, L. (1975). Decalcified, lyophilized bone allografts for use in human periodontal defects. *Journal of Periodontology, 46*, 51–56.

Lomas, R. J., Gillan, H. L., Matthews, J. B., Ingham, E., & Kearney, J. N. (2001). An evaluation of the capacity of differently prepared demineralized bone matrices (DBM) and toxic residuals of ethylene oxide (EtOx) to provoke an inflammatory response in vitro. *Biomaterials, 22*, 913–921.

Lozupone, E., & Favia, A. (1990). The structure of the trabeculae of cancellous bone. 2. Long bones and mastoid. *Calcified Tissue International, 46*, 367-372.

Marcott, C., Reeder, R. C., Paschalis, E. P., Tatakis, D. N., Boskey, A. L., & Mendelsohn, R. (1998). Infrared microspectroscopic imaging of biomineralized tissues using a mercury-cadmium-telluride focal-plane array detector. *Cellular and Molecular Biology, 44*(1), 109-115.

Martins, G., Freitas, J., Judas, F., Trindade, B., & Figueiredo, H. (2008). Evaluating Structural Differences in Cortical Bone Tissue After Demineralization and Calcination. *Microscopy and Microanalysis, 14*(S3), 162.

Miller, L. M., Vairavamurthy, V., Chance, M. R., Mendelsohn, R., Paschalis, E. P., Betts, F., et al. (2001). In situ analysis of mineral content and crystallinity in bone using infrared micro-spectroscopy of the ν4 PO43- vibration. *Biochimica et Biophysica Acta, 1527*(1-2), 11-19.

Mkukuma, L. D., Skakle, J. M. S., Gibson, I. R., Imrie, C. T., Aspden, R. M., & Hukins, D. W. L. (2004). Effect of the Proportion of Organic Material in Bone on Thermal Decomposition of Bone Mineral: An Investigation of a Variety of Bones from Different Species Using Thermogravimetric Analysis coupled to Mass Spectrometry, High-Temperature X-ray Diffraction, and Fourier Transform Infrared Spectroscopy. *Calcified Tissue International, 75*(4), 321-328.

Morone, M. A., & Boden, S. D. (1998). Experimental posterolateral lumbar spinal fusion with a demineralized bone matrix gel. *Spine, 23*, 159–167.

Murugan, R., Ramakrishna, S., & Rao, K. P. (2006). Nanoporous hydroxy-carbonate apatite scaffold made of natural bone. *Materials Letters, 60*, 2844–2847.

Murugan, R., Rao, K. P., & Kumar, T. S. S. (2003). Heat-deproteinated xenogeneic bone from slaughterhouse waste: physico-chemical properties. *Bulletin of Materials Science, 26*(5), 523–528.

Muyonga, J. H., Cole, C. G. B., & Duodu, K. G. (2004). Fourier transform infrared (FTIR) spectroscopic study of acid soluble collagen and gelatin from skins and bones of young and adult Nile perch (Lates niloticus). *Food Chemistry, 86*(3), 325-333

Nade, S., & Burwell, R. G. (1977). Decalcified bone as a substrate for osteogenesis: an appraisal of the interrelation of bone and marrow in combined grafts. *Journal of Bone Joint Surgery, 59-B*(2), 189–196.

Nudelman, F., Pieterse, K., George, A., Bomans, P. H. H., Friedrich, H., Brylka, L. J., et al. (2010). The role of collagen in bone apatite formation in the presence of hydroxyapatite nucleation inhibitors. *Nature Materials, 9*, 1004-1009.

Nyquist, R. A., Putzig, C. L., & Leugers, M. A. (1997). *The Handbook of Infrared and Raman Spectra of Inorganic Compounds and Organic Salts* (Vol. 1 and 4). San Diego, USA: Academic Press.

Olszta, M. J., Cheng, X., Jee, S. S., Kumar, R., Kim, Y. Y., Kaufman, M. J., et al. (2007). Bone structure and formation: A new perspective. *Materials Science and Engineering R 58*, 77-116.

Ooi, C., Hamdi, M., & Ramesh, S. (2007). Properties of hydroxyapatite produced by annealing of bovine bone. *Ceramics International, 33*(7), 1171-1177.

Ottani, V., Raspanti, M., & Ruggeri, A. (2001). Collagen structure and functional implications. *Micron, 32*, 251-260.

Paschalis, E. P., Betts, F., DiCarlo, E., Mendelsohn, R., & Boskey, A. L. (1997). FTIR microspectroscopic analysis of normal human cortical and trabecular bone. *Calcified Tissue International 61*, 480-486.

Paschalis, E. P., Mendelsohn, R., & Boskey, A. L. (2011). Infrared assessment of bone quality: a review. *Clinical Orthopaedics and Related Research, 469*(8), 2170-2178.

Paschalis, E. P., Recker, R., Di Carlo, E., Doty, S. B., Atti, E., & Boskey, A. L. (2003). Distribution of collagen cross-links in normal human trabecular bone. *Journal of Bone and Mineral Research, 18*(11).

Paschalis, E. P., Verdelis, K., Doty, S. B., Boskey, A. L., Mendelsohn, R., & Yamauchi, M. (2001). Spectroscopic characterization of collagen cross-links in bone. *Journal of Bone and Mineral Research, 16*(10).

Peterson, B., Whang, P. G., Iglesias, R., Wang, J. C., & Lieberman, R. J. (2004). Osteoinductivity of commercially available demineralized bone matrix. Preparations in a spine fusion model. *Journal of Bone Joint Surgery, 86*, 2243–2250.

Petibois, C., Wehbe, K., Belbachir, K., Noreen, R., & Déléris, G. (2009). Current Trends in the Development of FTIR Imaging for the Quantitative Analysis of Biological Samples. *Acta Physica Polonica A, 115*(2).

Pietrzak, W., Perns, S. V., Keyes, J., Woodell-May, J., & McDonald, N. (2005). Demineralized bone matrix graft: a scientific and clinical case study assessment. *Journal of Foot and Ankle Surgery, 44*, 345-353.

Pietrzak, W. S., Ali, S. N., Chitturi, D., Jacob, M., & Woodell-May, J. E. (2009). BMP depletion occurs during prolonged acid demineralization of bone: characterization and implications for graft preparation. *Cell and Tissue Banking, 12*(2), 81-88.

Rho, J.-Y., Kuhn-Spearing, L., & Zioupos, P. (1998). Mechanical properties and the hierarchical structure of bone. *Medical Engineering & Physics 20*, 92–102.

Robling, A. G., Castillo, A. B., & Turner, C. H. (2006). Biomechanical and Molecular Regulation of Bone Remodelling. *Annual Review of Biomedical Engineering, 8*, 455–498.

Roeges, N. P. G. (1994). *A guide to the complete interpretation of infrared spectra of organic structures*. Chichester, England: Wiley & Sons.

Rogers, K. D., & Daniels, P. (2002). An X-ray diffraction study of the effects of heat treatment on bone mineral microstructure. *Biomaterials, 23*, 2577–2585.

Saito, M., & Marumo, K. (2009). Collagen cross-links as a determinant of bone quality: a possible explanation for bone fragility in aging, osteoporosis, and diabetes mellitus. *Osteoporosis International, 21*(2), 195-214.

Shemesh, A. (1990). Crystallinity and diagenesis of sedimentary apatites. *Geochimica Et Cosmochimica Acta, 54*(9), 2433-2438.

Silva, L. d. M. S., Ebacher, V., Liu, D., McKay, H., Oxland, T. R., & Wang, R. (2005). Elasticity and Viscoelasticity of Human Tibial Cortical Bone Measured by Nanoindentation. *Materials Research Society Symposium Proceedings, 874*, L 5.8.1-L 5.8.6.

Torroni, A. (2009). Engineered Bone Grafts and Bone Flaps for Maxillofacial Defects: State of the Art. *Journal of Oral and Maxillofacial Surgery, 67*(5), 1121-1127.

Tzaphlidou, M. (2005). The role of collagen in bone structure: An image processing approach. *Micron, 36*(7-8), 593-601.

Urist, M. R. (1965). Bone formation by autoinduction. *Science, 150*, 893–899.

Verdelis, K. (2005). *Study of mineral and matrix maturation in dentin.* Ph.D. Dissertation, Faculty of North Carolina, Chapel Hill, USA.

Verdelis, K., Lukashova, L., Wright, J. T., Mendelsohn, R., Peterson, M. G. E., Doty, S., et al. (2007). Maturational changes in dentin mineral properties. *Bone, 40*(5), 1399-1407.

Viguet-Carrin, S., Follet, H., Gineyts, E., Roux, J. P., Munoz, F., Chapurlat, R., et al. (2010). Association between collagen cross-links and trabecular microarchitecture properties of human vertebral bone. *Bone, 46*(2), 342-347.

Viguet-Carrin, S., Garnero, P., & Delmas, P. D. (2005). The role of collagen in bone strength. *Osteoporosis International, 17*(3), 319-336.

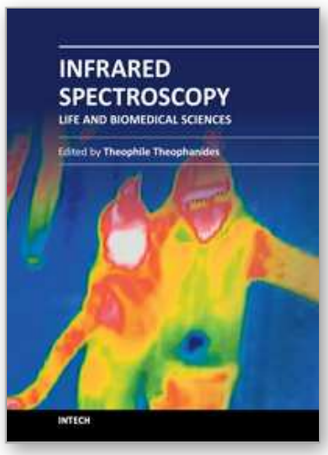

Infrared Spectroscopy - Life and Biomedical Sciences

Edited by Prof. Theophanides Theophile

ISBN 978-953-51-0538-1
Hard cover, 368 pages
Publisher InTech
Published online 25, April, 2012
Published in print edition April, 2012

This informative and state-of-the art book on Infrared Spectroscopy in Life sciences designed for researchers, academics as well as for those working in industry, agriculture and in pharmaceutical companies features 20 chapters of applications of MIRS and NIRS in brain activity and clinical research. It shows excellent FT-IR spectra of breast tissues, atheromatic plaques, human bones and projects assessment of haemodynamic activation in the cerebral cortex, brain oxygenation studies and many interesting insights from a medical perspective.

How to reference

In order to correctly reference this scholarly work, feel free to copy and paste the following:

M.M. Figueiredo, J.A.F. Gamelas and A.G. Martins (2012). Characterization of Bone and Bone-Based Graft Materials Using FTIR Spectroscopy, Infrared Spectroscopy - Life and Biomedical Sciences, Prof. Theophanides Theophile (Ed.), ISBN: 978-953-51-0538-1, InTech, Available from: http://www.intechopen.com/books/infrared-spectroscopy-life-and-biomedical-sciences/characterization-of-bone-and-bone-based-graft-materials-using-ftir-spectroscopy

INTECH
open science | open minds

InTech Europe
University Campus STeP Ri
Slavka Krautzeka 83/A
51000 Rijeka, Croatia
Phone: +385 (51) 770 447
Fax: +385 (51) 686 166
www.intechopen.com

InTech China
Unit 405, Office Block, Hotel Equatorial Shanghai
No.65, Yan An Road (West), Shanghai, 200040, China
中国上海市延安西路65号上海国际贵都大饭店办公楼405单元
Phone: +86-21-62489820
Fax: +86-21-62489821

IntechOpen